Chemical Engineering Journal 99 (2004) 105–116

Chemical Engineering Journal

www.elsevier.com/locate/cej

Effectiveness factor for zeolite catalysed isomerization reactions

R. Baur, R. Krishna*

Department of Chemical Engineering, University of Amsterdam, Nieuwe Achtergracht 166, Amsterdam 1018 WV, The Netherlands

Received 16 June 2003; accepted 20 September 2003

Abstract

We analyze the influence of diffusion on the reversible isomerization reaction $A_1 \leftrightarrow A_2$, occurring within a zeolite catalyst, of spherical, cylindrical, and slab geometries. The intra-crystalline diffusion process is described by the Maxwell–Stefan (M–S) equations. Two different guest–host *confinement* scenarios are examined. For *strongly confined* guest molecules, the M–S diffusivities $Đ_i$ decrease with loading inside the zeolite. For weakly confined guest molecules, the M–S diffusivities $Đ_i$ are independent of the loading. The correlation effects, typical of zeolite diffusion, are described by introducing an *exchange* coefficient $Đ_{12}$ in the M–S diffusion formulation. For *facile* exchange, $Đ_{12\to\infty}$, correlation effects are washed out. For *finite* exchange, a logarithmic interpolation formula is used to calculate $Đ_{12}$ from the two *pure* component M–S diffusivities $Đ_i$. Analytic expressions for the effectiveness factor are derived for a variety of *confinement* and *exchange* scenarios. In the development of the analytic solution we assume Langmuirian behavior of the pure components and that the mixture sorption loadings can be calculated from the multicomponent Langmuir isotherm. By means of a variety of numerical examples, we stress the various characteristic features of intra-crystalline diffusion influences in zeolite catalysis. The effectiveness factor is found to a strong function of (a) molecular loadings and mixture composition, (b) ratio of diffusivities of the participating species, and (c) the reaction equilibrium constant. Only for the case of low loadings of weakly confined guest molecules and vanishing correlation effects, is the classical formula for the effectiveness factor valid.

Keywords: Maxwell–Stefan theory; Zeolite catalysis; Isomerization; Effectiveness factor; Correlation effects; Confinement effects

1. Introduction

Zeolites are widely used in the processing industries to catalyze a variety of reactions such as cracking, oxidation, isomerization, and alkylation [1–5]. From a practical point of view it is necessary to describe the influence of intra-crystalline diffusion on the chemical reaction. The description of the diffusion process is complicated by the fact that there are more than 100 different zeolite structures available [6]. Viewed simply, these structures fall into three broad categories: (a) structures with intersecting channels, (b) cages-separated-by-windows, and (c) essentially cylindrical channels, sometimes with side "pockets"; see Fig. 1. The diffusivities are strongly dependent on the pore size and zeolite topology. Depending on the guest–host combination, zeolite diffusivities show a variety of dependencies on the molecular loading [1,2,7–11]. Correlation effects on diffusion need to be considered; these effects are influenced inter alia by zeolite topology and connectivity [10,12].

There are very few publications that analyze diffusion and chemical reaction within zeolite catalysts. One of the first analyses of diffusion-reaction in zeolite catalysts was by Ruthven [13] who considered an irreversible reaction, with the product exiting the reaction zone instantaneously. Theodorou and Wei [14] analyzed a first-order isomerisation reaction in a two-dimensional lattice, assuming the two species to have identical diffusivities. Sundaresan and Hall [15] used a lattice model to examine the influence of pore blocking on reactivity.

The major objective of this paper is to describe the influence of diffusion on zeolite catalysis in a generic manner that is valid for a variety of zeolite topologies and guest–host combinations. We use the Maxwell–Stefan (M–S) formulation [16–20] for describing zeolite diffusion. In order to develop *analytic* solutions for the effectiveness factor, we restrict our analysis to a reversible isomerization reaction $A_1 \leftrightarrow A_2$. Such isomerization reactions are of great significance to the petroleum industry [3–5].

* Corresponding author. Tel.: +31-20-5257007; fax: +31-20-5255604.
E-mail address: krishna@science.uva.nl (R. Krishna).

1385-8947/$ – see front matter © 2003 Elsevier B.V. All rights reserved.
doi:10.1016/j.cej.2003.09.007

Nomenclature

List of symbols

b_i	parameter in the pure component Langmuir adsorption isotherm (Pa^{-1})
$[B]$	square matrix with elements defined by Eq. (9) ($m^{-2}\,s$)
$Đ_i(0)$	M–S diffusivity of species i at zero loading ($m^2\,s^{-1}$)
$Đ_i$	M–S diffusivity of species i ($m^2\,s^{-1}$)
$Đ_{12}$	exchange M–S diffusivity describing interchange between i and j ($m^2\,s^{-1}$)
k_1	forward reaction rate constant (s^{-1})
k_2	backward reaction rate constant (s^{-1})
N_i	molar flux of species i ($mol\,m^{-2}\,s^{-1}$)
p_i	partial pressure of species i (Pa)
q_i	molar loading of component i ($mol\,kg^{-1}$)
q_{sat}	saturation loading ($mol\,kg^{-1}$)
r	reaction rate (s^{-1})
R	gas constant ($8.314\,J\,mol^{-1}\,K^{-1}$)
T	absolute temperature (K)
z	distance along diffusion path in crystal (m)

Greek letters

β	$\beta \equiv \sqrt{\{(Đ_2(0)/Đ_1(0))[\Lambda(k_1/k_2)+1)]\}/\Lambda[(Đ_2(0)/Đ_1(0))(k_1/k_2)+1]}$ (dimensionless parameter)
χ	parameter defined by Eq. (C.2) (dimensionless)
δ	characteristic distance of zeolite crystal; half thickness of slab, radius of spherical or cylindrical catalyst (m)
ϕ	Thiele modulus, $\phi \equiv (\delta/\zeta)\sqrt{(k_1/Đ_1(0)) + (k_2/Đ_2(0))}$ (dimensionless)
Φ	modified Thiele modulus; see Table 1 (dimensionless)
γ	confinement parameter; $\gamma = 0$ for weak, $\gamma = 1$ for strong (dimensionless)
η	effectiveness factor (dimensionless)
π_i	dimensionless partial pressures, $b_i p_i$ (dimensionless)
μ_i	molar chemical potential ($J\,mol^{-1}$)
ν_i	reaction stoichiometric coefficient; $\nu_1 = 1$ for reactant A_1; $\nu_2 = -1$ for product A_2
θ_i	fractional occupancy of component i, $\theta_i = q_i/q_{sat}$ (dimensionless)
θ_{is}	fractional occupancy at catalyst surface (dimensionless)
θ_{i0}	fractional occupancy at center of catalyst (dimensionless)
θ_V	fractional vacancy, $\theta_V = 1 - \theta_1 - \theta_2$ (dimensionless)
Θ	$\Theta \equiv (\sqrt{2(1-(1/\Psi^2) - (2\ln(\Psi)/\Psi^2))})/(\lvert 1-(1/\Psi^2)\rvert)$ (dimensionless parameter)
ρ	density of zeolite ($kg\,m^{-3}$)
ω	$\omega = ((k_1+k_2)\theta_{1s})/(k_2(1-\theta_{Vs}))$ (dimensionless parameter)
ξ	dimensionless distance along catalyst; $\xi = 0$ (center), $\xi = 1$ (surface)
Ψ	$\Psi \equiv \sqrt{[(\Lambda + (1-\Lambda)\theta_{1s})k_1 + (1+(\Lambda-1)\theta_{2s})k_2]/(\Lambda k_1 + k_2)}$ (dimensionless parameter)
ζ	$\zeta = 1$ for slab, $\zeta = 2$ for cylinder, $\zeta = 3$ for sphere (geometry parameter)
Ξ	$\Xi \equiv \sqrt{(1/\theta_{Vs}^{\gamma})\{1 + [(\theta_{1s}+\theta_{2s})(Đ_1(0)/Đ_{12}(0))]\}}$
Λ	dimensionless diffusivity ratio, $\Lambda \equiv (Đ_2(0)/Đ_1(0))[1 + (\theta_{1s}+\theta_{2s})(Đ_1(0)/Đ_{12}(0))]/[1 + (\theta_{1s}+\theta_{2s})(Đ_2(0)/Đ_{12}(0))]$

Subscripts

0	referring to surface at center of catalyst, $\xi = 0$
1	referring to species 1
2	referring to species 2
i	referring to species i
s	referring to surface at position $\xi = 1$
sat	referring to saturation conditions
V	vacancy
ξ	at position ξ within catalyst

Vector and matrix notation

( )	component vector
[ ]	square matrix

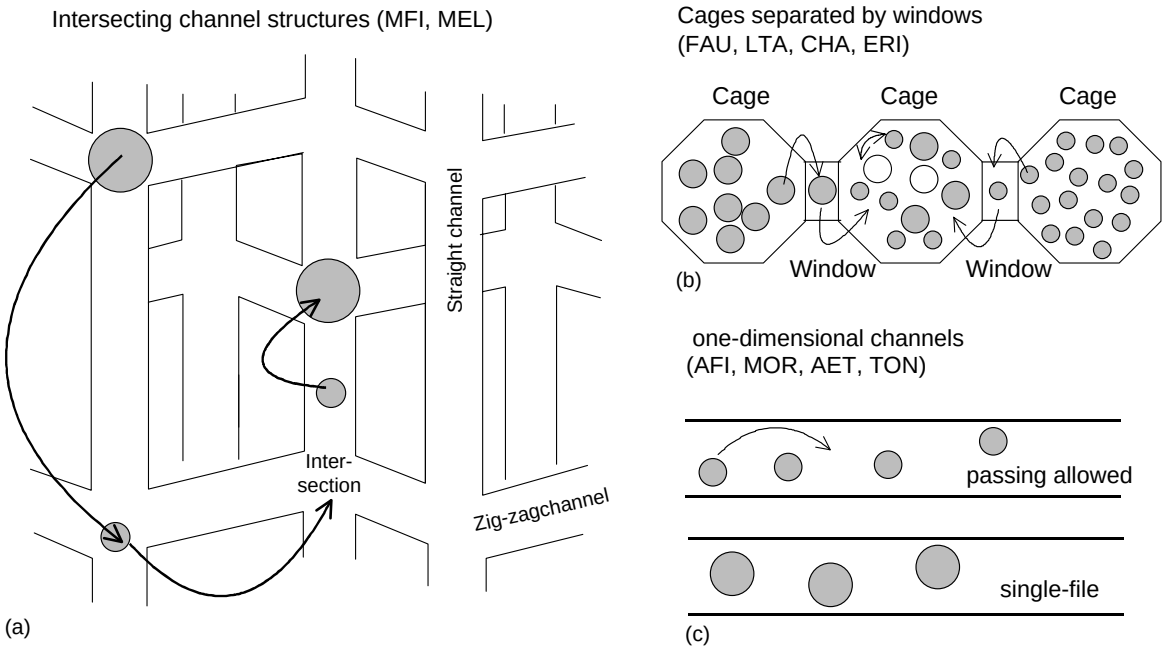

Fig. 1. Pictorial representation of the molecular jumps in: (a) intersecting channel structures, (b) cages separated by windows, and (c) single file diffusion in one-dimensional channels.

2. The Maxwell–Stefan formulation for zeolite diffusion

In the M–S formulation, the chemical potential gradients are written as linear functions of the fluxes [16–20]:

$$-\frac{\rho q_{\mathrm{sat}}}{\delta}\frac{\theta_1}{RT}\frac{\partial \mu_1}{\partial \xi} = \frac{\theta_2 N_1 - \theta_1 N_2}{Đ_{12}} + \frac{N_1}{Đ_1},$$
$$-\frac{\rho q_{\mathrm{sat}}}{\delta}\frac{\theta_2}{RT}\frac{\partial \mu_2}{\partial \xi} = \frac{\theta_1 N_2 - \theta_2 N_1}{Đ_{12}} + \frac{N_2}{Đ_2} \quad (1)$$

where the fractional occupancies θ_i serve as replacements for mole fractions used for description of bulk fluid phase diffusion. In this paper, we consider three different geometries of zeolite crystals, as shown in Fig. 2.

We have to reckon in general with two types of Maxwell–Stefan diffusivities: $Đ_i$ and $Đ_{12}$. The $Đ_i$ are the diffusivities that reflect interactions between species i and the zeolite matrix; they are also referred to as jump or "corrected" diffusivities in the zeolite literature [1,2]. Experimental and molecular dynamics (MD) simulation data for weakly confined guest molecules in zeolitic hosts (e.g. methane, He, Ne, Ar in MFI) show that $Đ_i$ are practically independent of the loading, i.e. occupancy [7–9,18,21].

$$Đ_i = Đ_i(0) \quad (2)$$

For diffusion of larger guest molecules, such as CF_4, SF_6, and 2-methylhexane (2MH) in MFI a different loading dependence of $Đ_i$ has been observed in MD [9,10] and Kinetic Monte Carlo (KMC) simulations [22–24]. These studies show that $Đ_i$ decreases strongly with the loading and follows the relation

$$Đ_i = Đ_i(0)\theta_{\mathrm{V}} \quad (3)$$

where θ_{V} is the vacancy, $\theta_{\mathrm{V}} = 1 - \theta_1 - \theta_2$. By defining a confinement parameter γ ($\gamma = 1$ for strong, $\gamma = 0$ for weak), we may write the following general expression for the occupancy dependence of the M–S diffusivity:

$$Đ_i = Đ_i(0)\theta_{\mathrm{V}}^{\gamma} \quad (4)$$

Whether a molecule follows scenario (2) or (3) depends also on adsorbate–adsorbate interactions [9,12,25] and zeolite topology [11]. The loading dependence can also lie intermediate between the weak and strong confinement scenarios [10].

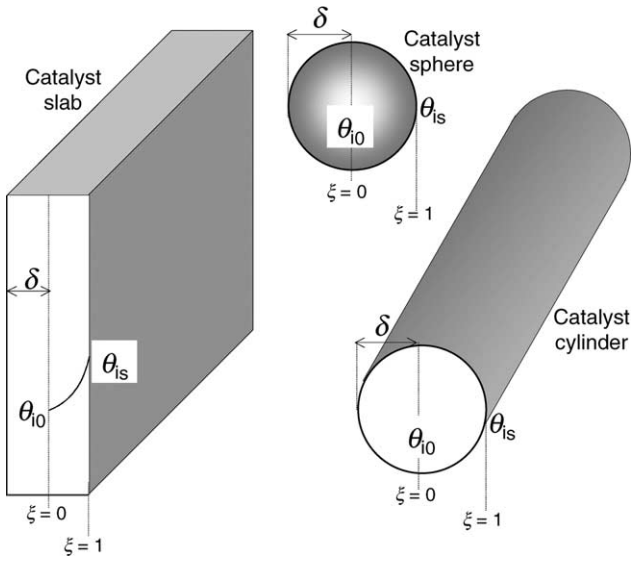

Fig. 2. Three different zeolite catalyst geometries considered in this work.

Fig. 1 portrays the molecular jump processes in: (a) intersecting channel structures, (b) cage-type structures, separated by windows, and (c) single-file diffusion diffusion in one-dimensional channels. Site-to-site jump leaves behind a vacancy. Subsequent jumps are more likely to fill this vacancy, thus producing "vacancy correlation" effects [12,26]. When the jump of species i creates a vacancy and this vacancy is filled by species j, the vacancy correlation effect is captured by the term containing the "exchange" coefficients $Đ_{12}$ in Eq. (1). The Onsager reciprocal relations demand $Đ_{12} = Đ_{21}$. The net effect of this exchange is a slowing down of a faster moving species due to interactions with a species of lower mobility. Also, a species of lower mobility is accelerated by interactions with another species of higher mobility.

For estimation of the $Đ_{12}$, Krishna and Wesselingh [16] suggested the logarithmic interpolation formula:

$$Đ_{12} = [Đ_1(0)]^{\theta_1/(\theta_1+\theta_2)}[Đ_2(0)]^{\theta_2/(\theta_1+\theta_2)}\theta_V^{\gamma} \equiv Đ_{12}(0)\theta_V^{\gamma} \tag{5}$$

The interpolation strategy (5) has been verified by comparison with Monte Carlo and molecular dynamics simulations [26,27]. For zeolite topologies with high connectivities, the exchange coefficient $Đ_{12}$ can be expected to be high, as has been shown by Skoulidas et al. [10]. For facile particle–particle exchange, i.e. $Đ_{12} \to \infty$, vacancy correlation effects tend to get washed out.

We assume that the individual component loadings follow the multicomponent Langmuir isotherm

$$\theta_i = \frac{q_i}{q_{sat}} = \frac{b_i p_i}{1 + b_1 p_1 + b_2 p_2} \equiv \frac{\pi_i}{1 + \pi_1 + \pi_2} \equiv \theta_V \pi_i; \quad i = 1, 2 \tag{6}$$

where we define the dimensionless pressures $\pi_i \equiv b_i p_i$. The chemical potential gradients in Eq. (1) may be expressed in terms of the gradients of the occupancies by expressing the chemical potential gradients in terms of the (dimensionless) partial pressure gradients

$$\frac{\theta_i}{RT}\frac{\partial \mu_i}{\partial \xi} = \frac{\theta_i}{p_i}\frac{\partial p_i}{\partial \xi} = \theta_V \frac{\partial \pi_i}{\partial \xi}; \quad i, j = 1, 2 \tag{7}$$

Eq. (1) may be recast into n-dimensional matrix expressing the fluxes explicitly in terms of the dimensionless pressure gradients

$$(N) = -\frac{\rho q_{sat}}{\delta}[B]^{-1}\theta_V^{\gamma+1}\frac{\partial \pi}{\partial \xi} \tag{8}$$

where we define the n-dimensional square matrix $[B]$ with elements

$$B_{11} = \frac{1}{Đ_1(0)} + \frac{\theta_2}{Đ_{12}(0)}; \qquad B_{12} = -\frac{\theta_1}{Đ_{12}(0)};$$
$$B_{22} = \frac{1}{Đ_2(0)} + \frac{\theta_1}{Đ_{12}(0)}; \quad B_{21} = -\frac{\theta_2}{Đ_{12}(0)} \tag{9}$$

The elements of the matrix $[B]$ are dependent on the molecular occupancies within the zeolite. In the analytic solutions to be developed below, we evaluate the matrix $[B]$ at the conditions prevailing on the *surface* of the catalyst, i.e. at loadings θ_{is} and assume $[B]$ to be ξ-invariant. This assumption will be validated subsequently by comparing the analytic solutions with precise numerical solutions wherein the occupancy dependence of $[B]$ is accounted for in a precise manner.

Rearranging Eq. (8):

$$\sum_{j=1}^{2} B_{ij}\frac{N_j \delta}{\rho q_{sat}} = -\theta_V^{\gamma+1}\left(\frac{\partial \pi_i}{\partial \xi}\right); \quad i = 1, 2 \tag{10}$$

and summing Eq. (10) over both species and introducing $(\pi_1 + \pi_2) \equiv (1/\theta_V) - 1$:

$$\sum_{i=1}^{2}\sum_{j=1}^{2} B_{ij}\frac{\delta}{\rho}\frac{N_i}{q_{sat}} = -\theta_V^{\gamma+1}\frac{\partial(\pi_1 + \pi_2)}{\partial \xi} = -\theta_V^{\gamma-1}\frac{\partial \theta_V}{\partial \xi} \tag{11}$$

Introducing the elements B_{ij} from Eq. (9), we note that the off-diagonal terms drop out in the double summation on the left member of Eq. (11) to yield

$$\sum_{i=1}^{n}\frac{N_i \delta}{\rho q_{sat} Đ_i(0)} = -\theta_V^{\gamma-1}\frac{\partial \theta_V}{\partial \xi}. \tag{12}$$

3. Effectiveness factor

The differential equations describing the diffusion and reversible isomerization reaction $A_1 \leftrightarrow A_2$ within the three zeolite catalyst geometries considered in Fig. 2 are:

$$\frac{1}{\delta \xi^{\zeta-1}}\frac{\partial}{\partial \xi}(\xi^{\zeta-1} N_i) = \rho q_{sat} \nu_i r; \quad i = 1, 2 \tag{13}$$

where the stoichiometric coefficients $\nu_1 = 1$ for reactant A_1 and $\nu_2 = -1$ for product A_2. For Langmuir–Hinshelwood kinetics, the reaction rate r is

$$r = \frac{k_1 b_1 p_1 - k_2 b_2 p_2}{1 + b_1 p_1 + b_2 p_2} \equiv k_1\theta_1 - k_2\theta_2 \equiv \theta_V(k_1\pi_1 - k_2\pi_2) \tag{14}$$

The outer surface of the catalyst ($\xi = 1$) is in equilibrium with the bulk fluid phase:

$$\xi = 1: \quad p_i = p_{is}; \quad q_i = q_{is}; \quad \theta_i = \theta_{is}; \quad \pi_i = \pi_{is}; \quad \theta_V = \theta_{Vs} \tag{15}$$

At the center of the catalyst, the fluxes, and gradients, vanish:

$$\xi = 0: \quad N_{i0} = 0; \quad \left.\frac{\partial \theta_i}{\partial \xi}\right|_{\xi=0} = 0; \quad \left.\frac{\partial \theta_V}{\partial \xi}\right|_{\xi=0} = 0 \tag{16}$$

Substituting Eq. (14) into Eq. (13) we obtain after rearrangement

$$\frac{1}{\delta^2\xi^{\zeta-1}}\frac{\partial}{\partial\xi}\left(\xi^{\zeta-1}\theta_V^{\gamma+1}\sum_{j=1}^{2}B_{ij}^{-1}\frac{\partial\pi_j}{\partial\xi}\right)=-\nu_i r;\quad i=1,2 \tag{17}$$

Integrating Eq. (17) once we obtain

$$\frac{1}{\nu_i}\sum_{j=1}^{2}B_{i,j}^{-1}\frac{\partial\pi_j}{\partial\xi}=-\frac{\delta^2}{\xi^{\zeta-1}\theta_V^{\gamma+1}}\int_1^{\xi}\xi^{\zeta-1}r(\xi)\,\mathrm{d}\xi \tag{18}$$

The right member of Eq. (18) is *i*-invariant. Hence, we may inter-relate the partial pressure gradients of components 1 and 2:

$$\frac{1}{\nu_1}\sum_{j=1}^{2}B_{1,j}^{-1}\frac{\partial\pi_j}{\partial\xi}=\frac{1}{\nu_2}\sum_{j=1}^{2}B_{2,j}^{-1}\frac{\partial\pi_j}{\partial\xi} \tag{19}$$

Simplifying Eq. (19) we obtain:

$$\frac{\partial\pi_1}{\partial\xi}=-\frac{\mathcal{D}_2(0)[1+(\theta_{1s}+\theta_{2s})(\mathcal{D}_1(0)/\mathcal{D}_{12}(0))]}{\mathcal{D}_1(0)[1+(\theta_{1s}+\theta_{2s})(\mathcal{D}_2(0)/\mathcal{D}_{12}(0))]}\frac{\partial\pi_2}{\partial\xi}\equiv-\Lambda\frac{\partial\pi_2}{\partial\xi} \tag{20}$$

Integrating Eq. (20) we obtain the partial pressure and occupancy profiles in terms of the vacancy profile $\theta_V(\xi)$ and the occupancies at the surface of the catalyst ($\xi=1$), i.e. θ_{is}, that are known.

$$\pi_1=\frac{\Lambda}{(\Lambda-1)\theta_V}-\frac{\Lambda\theta_{Vs}+\theta_{1s}+\Lambda\theta_{2s}}{(\Lambda-1)\theta_{Vs}};\qquad \theta_1=\frac{\Lambda}{(\Lambda-1)}-\frac{\Lambda\theta_{Vs}+\theta_{1s}+\Lambda\theta_{2s}}{(\Lambda-1)\theta_{Vs}}\theta_V \tag{21}$$

$$\pi_2=\frac{1}{(1-\Lambda)\theta_V}-\frac{\Lambda\theta_{2s}+\theta_{Vs}+\theta_{1s}}{(1-\Lambda)\theta_{Vs}};\qquad \theta_2=\frac{1}{(1-\Lambda)}-\frac{\Lambda\theta_{2s}+\theta_{Vs}+\theta_{1s}}{(1-\Lambda)\theta_{Vs}}\theta_V \tag{22}$$

With Eqs. (21) and (22), the reaction rate can be expressed purely in terms of the vacancy $\theta_V(\xi)$ and the occupancies at the surface:

$$r=\frac{\Lambda k_1+k_2}{(\Lambda-1)}\left(1-\Psi^2\frac{\theta_V}{\theta_{Vs}}\right);\qquad \Psi\equiv\sqrt{\frac{(\Lambda+(1-\Lambda)\theta_{1s})k_1+(1+(\Lambda-1)\theta_{2s})k_2}{(\Lambda k_1+k_2)}} \tag{23}$$

Evaluating the elements of the matrix [*B*] at the surface occupancies, θ_{is}, and assuming these to be constant we may re-write Eq. (17) as

$$\frac{1}{\delta^2\xi^{\zeta-1}}\frac{\partial}{\partial\xi}\left(\xi^{\zeta-1}\theta_V^{\gamma+1}\frac{\partial\pi_i}{\partial\xi}\right)=-\sum_{j=1}^{2}B_{ij}\nu_j r;\quad i=1,2 \tag{24}$$

Replacing partial pressure gradients with vacancy gradients using Eqs. (21) and (22), we obtain a *single* differential equation in terms of the vacancy gradients

$$\frac{1}{\xi^{\zeta-1}}\frac{\partial}{\partial\xi}\left(\xi^{\zeta-1}\left(\frac{\theta_V}{\theta_{Vs}}\right)^{\gamma-1}\frac{\partial(\theta_V/\theta_{Vs})}{\partial\xi}\right)=(\zeta\phi\beta\Xi\Psi)^2\left(\frac{\theta_V}{\theta_{Vs}}-\frac{1}{\Psi^2}\right) \tag{25}$$

subject to the boundary conditions given by Eqs. (15) and (16). The parameter ϕ is the classical Thiele modulus

$$\phi\equiv\frac{\delta}{\zeta}\sqrt{\frac{k_1}{\mathcal{D}_1(0)}+\frac{k_2}{\mathcal{D}_2(0)}} \tag{26}$$

The dimensionless parameters β and Ξ are defined in the Nomenclature section. Analytic solutions to Eq. (25) can be derived for various special cases as shown in the Appendix A (strong confinement), Appendix B (equal diffusivities), and Appendix C (weak confinement). These analytic solutions are exact only for: (1) facile exchange and strong confinement; (2) facile exchange and equal diffusivities. For the weak confinement scenario with facile exchange the analytic solution is exact only for the limiting cases of $\phi\to\infty$ and $\phi\to 0$. We show below, by comparing with precise numerical solutions that the presented analytic solutions are excellent approximations for both confinement scenarios, even for finite exchange, for a wide range of Thiele modulii ϕ. The solutions for the vacancy profile $\theta_V(\xi)$ and effectiveness factor η are *formally* identical to the classical solutions [28]:

$$\frac{\theta_V}{\theta_{Vs}}=\frac{1}{\Psi^2}+\left(\frac{\Psi^2-1}{\Psi^2}\right)\frac{\cosh(\Phi\xi)}{\cosh(\Phi)};\quad \text{slab}(\zeta=1)$$
$$\frac{\theta_V}{\theta_{Vs}}=\frac{1}{\Psi^2}+\left(\frac{\Psi^2-1}{\Psi^2}\right)\frac{I_0(2\Phi\xi)}{I_0(2\Phi)};\quad \text{cylinder}(\zeta=2)$$
$$\frac{\theta_V}{\theta_{Vs}}=\frac{1}{\Psi^2}+\left(\frac{\Psi^2-1}{\Psi^2}\right)\frac{\sinh(3\Phi\xi)}{\sinh(3\Phi)};\quad \text{sphere}(\zeta=3) \tag{27}$$

and

$$\eta=\frac{\tanh(\Phi)}{\Phi};\quad \text{slab}(\zeta=1)$$
$$\eta=\frac{I_1(2\Phi)}{\Phi I_0(2\Phi)};\quad \text{cylinder}(\zeta=2) \tag{28}$$
$$\eta=\frac{1}{\Phi}\left(\frac{1}{\tanh(3\Phi)}-\frac{1}{3\Phi}\right);\quad \text{sphere}(\zeta=3)$$

where we define a *generalized* Thiele modulus Φ, that is related to the *classical* Thiele modulus ϕ in different ways depending on the specific scenarios; these are specified in Table 1. For all three geometries, the effectiveness factor yields the limiting value

$$\eta=\frac{1}{\Phi} \tag{29}$$

Table 1
Calculation of modified Thiele modulus for various scenarios

Scenario	Formula for modified Thiele modulus	Remarks about analytic solution
Equal diffusivities: $\mathcal{Đ}_1(0) = \mathcal{Đ}_2(0)$	$\Phi = \phi\Xi$	Exact
Strong confinement	$\Phi = \phi\beta\Xi\Psi$	Exact for facile exchange; for finite exchange, a very good approximation
Weak confinement	$\Phi = (\phi\beta\Xi\Psi/\Theta)$	Exact for facile exchange in the limiting cases $\phi \to \infty$ and $\phi \to 0$; for all other cases, including that for finite exchange, a very good approximation

for large values of the modified Thiele modulus Φ, and low values of the effectiveness factor say. Eq. (29) represents a classical result that is well entrenched in the chemical reaction engineering literature [28].

Occupancies of the individual components can be obtained by combining Eq. (27) with Eqs. (21) and (22).

4. Illustrative examples

We shall illustrate the many peculiarities of zeolite diffusion by means of several illustrative examples. Let us first consider the special case in which the diffusivities of the two components A_1 and A_2 participating in the isomerization reaction $A_1 \leftrightarrow A_2$ are equal, i.e. $\mathcal{Đ}_1(0) = \mathcal{Đ}_2(0)$. For the case of equal diffusivities, the total vacancy is constant along the diffusion path, as shown in Appendix B. The fractional occupancy of component A_1 is given by Eq. (B.5) of Appendix B, represented by continuous lines in Fig. 3a taking $k_1 = 2k_2$; $\phi = 1.1547$; $\theta_{1s} = 0.6$; $\theta_{2s} = 0.2$. Both weak and strong confinement scenarios, with either facile $\mathcal{Đ}_{12}(0) \to \infty$ or finite exchange (following Eq. (5)) are considered in the calculations. The profiles for the fractional occupancy of component A_2 is related to that for component A_1, i.e. $\theta_2 = 1 - \theta_1 - \theta_{Vs}$. The different symbols in Fig. 3a represent precise numerical solutions using the numerical methods described on our website: http://ct-cr4.chem.uva.nl/zeolites/. In the numerical approach, the partial differential equations are discretized using a finite volume discretization and the entire set of equations is solved using a sparse matrix DAE solver as described by Kooijman [29]. For all the four cases shown there is excellent agreement between the analytic solutions and the numerical solutions. For facile exchange, the analytic solutions are exact and we should expect precise agreement between the analytic and numerical solutions. For finite exchange, the key assumption made in the derivation of the analytic solution is that the elements of the matrix $[B]$ is constant along the diffusion path and can be evaluated from the (known) surface occupancies, θ_{is}. The excellent agreement between the numerical and analytic solutions for finite exchange testifies to the validity of the key assumption.

The effectiveness factor η is plotted in Fig. 3b as a function of the classical Thiele modulus ϕ for both weak and strong confinement, with either facile $\mathcal{Đ}_{12}(0) \to \infty$ or finite exchange (following Eq. (5)). The continuous lines are the calculations for a spherical catalyst using Eq. (28), taking $\Phi = \phi\Xi$. The factor Ξ serves to "correct" the classical Thiele modulus ϕ to take account of confinement and exchange effects.

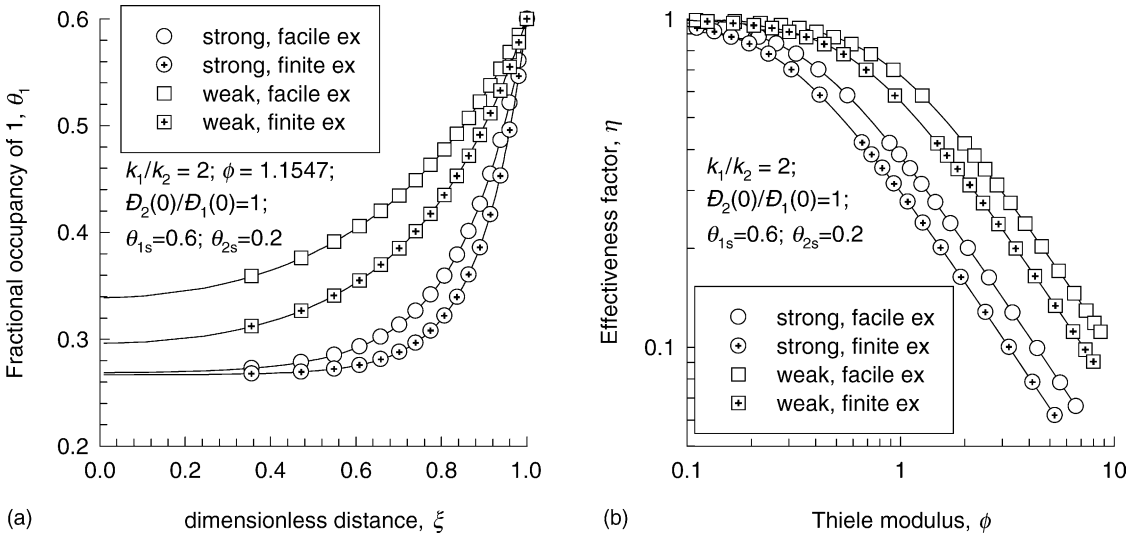

Fig. 3. (a) Fractional occupancy profiles for component 1, θ_1, along the diffusion path in a spherical catalyst for $\phi = 1.1547$, and (b) effectiveness factor η vs. classical Thiele modulus ϕ, for equal diffusivities of the two species $\mathcal{Đ}_1(0) = \mathcal{Đ}_2(0)$. Other parameters are $k_1 = 2k_2$; $\theta_{1s} = 0.6$; $\theta_{2s} = 0.2$. Symbols represent precise numerical solutions obtained using the numerical techniques described on our website: http://ct-cr4.chem.uva.nl/zeolites/. The continuous lines in parts (a) and (b) are drawn using Eqs. (B.5) and (28), respectively), with definitions of Φ as in Table 1.

For facile exchange of weakly confined molecules, the "correction" factor $\Xi \equiv 1$, and therefore η for this case coincides with the classical case. Finite exchange tends to *reduce* η. The effectiveness for strong confinement is significantly lower than for the corresponding weak confinement case; this is because of the fact that the M–S diffusivities decrease with loading following Eq. (3).

One of the key features of zeolite diffusion is the influence of occupancies of the species on the diffusivities, and consequently on the effectiveness factor. In order to highlight this influence, we consider diffusion-reaction within a catalyst of slab geometry, with a fixed classical Thiele modulus value $\phi = 0.6841$. For equal diffusivities of the two species participating in the isomerization reaction, effectiveness factor calculated using Eq. (28) are shown in Fig. 4 for four different scenarios of confinement and exchange.

For facile exchange of weakly confined molecules, the "correction" factor $\Xi \equiv 1$, and therefore η for this case coincides with the classical case and effectiveness factor is independent of occupancy, having a constant value of 0.8. For finite exchange, caused by correlation effects, the "correction" factor, $\Xi \equiv \sqrt{1+\theta_{1s}+\theta_{2s}} = \sqrt{1+\theta_1+\theta_2}$ for weak confinement and we note the slight decrease of η with total occupancy. For strong confinement with facile exchange $\Xi = \sqrt{1/(1-\theta_1-\theta_2)}$ and η decreases sharply as the total occupancy increases; these calculations are in good agreement with the Kinetic Monte Carlo simulations of Theodorou and Wei [14] obtained for isomerization diffusion-reaction with strong confinement in a two-dimensional lattice for $\phi = 0.6841$. The two-dimensional lattice has a high enough connectivity value to ensure a high exchange coefficient $Đ_{12}$ to allow the facile exchange scenario to hold. With finite exchange, of strongly confined molecules the correction factor $\Xi = \sqrt{(1+\theta_1+\theta_2)/(1-\theta_1-\theta_2)}$ and the η is significantly lower than for the corresponding case with facile exchange.

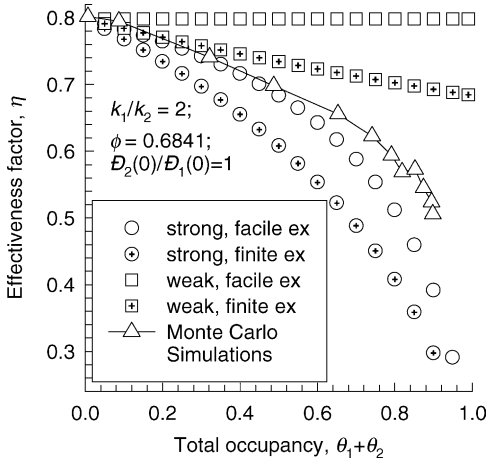

Fig. 4. Effectiveness factor η vs. total occupancy, for equal diffusivities of the two species $Đ_1(0) = Đ_2(0)$ for the slab catalyst geometry for four different scenarios. Other parameters are $k_1 = 2k_2$; $\phi = 0.6841$. The effectiveness factors are calculated using Eq. (28). Also plotted are the Kinetic Monte Carlo simulations of Theodorou and Wei [14] obtained in a two-dimensional lattice.

Let us examine now the case for which the diffusivity of species A_2 is 100 times smaller than that of A_1. This situation can arise for alkane isomerization where due to a higher degree of branching of A_2 its diffusivity is significantly reduced. The vacancy profiles for a spherical catalyst with $\phi = 0.6733$, are shown in Fig. 5a with continuous lines calculated using Eq. (27) for four different scenarios. As in the case for equal diffusivities, there is excellent agreement between the analytic solutions and precise numerical solutions (indicated with symbols). Interestingly for this case

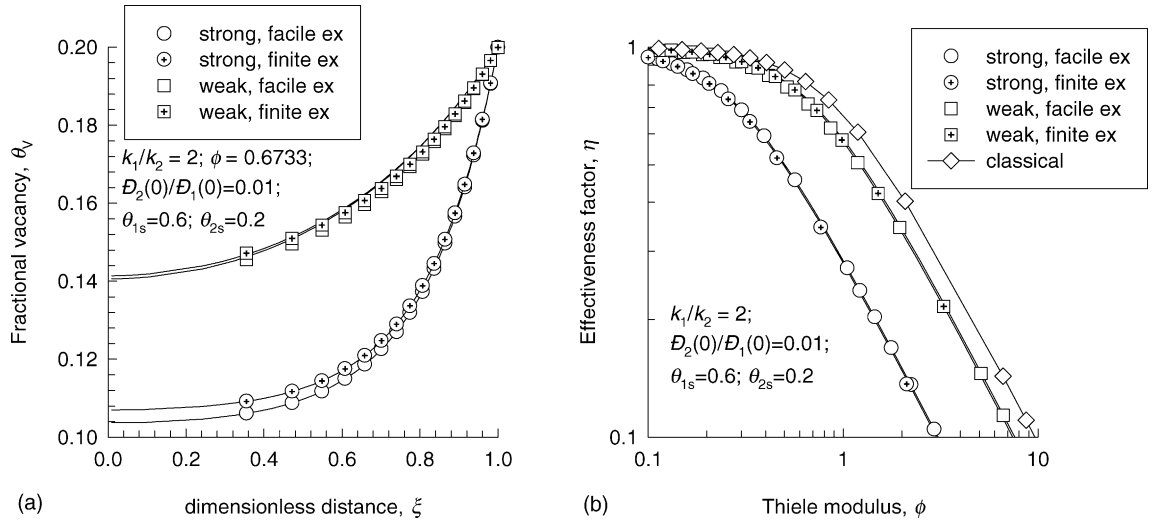

Fig. 5. (a) Fractional vacancy profile along the diffusion path in a spherical catalyst for $\phi = 0.6733$, and (b) effectiveness factor η vs. classical Thiele modulus ϕ. Other parameters are $Đ_2(0) = Đ_1(0) = 0.01$; $k_1 = 2k_2$; $\theta_{1s} = 0.6$; $\theta_{2s} = 0.2$. Symbols represent precise numerical solutions obtained using the numerical techniques described on our website: http://ct-cr4.chem.uva.nl/zeolites/. The continuous lines in parts (a) and (b) are drawn using Eqs. (27) and (28), respectively), with definitions of Φ as in Table 1.

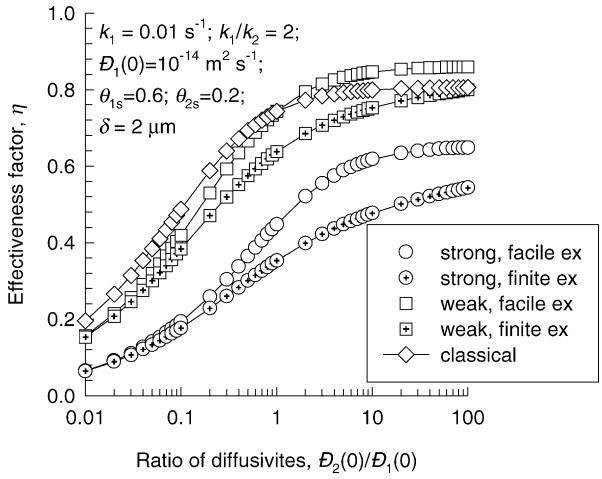

Fig. 6. Effectiveness factor η for varying diffusivity ratios. Other parameters for the spherical catalyst geometry are $k_1 = 0.01\,s^{-1}$; $k_1 = 2k_2$; $\theta_{1s} = 0.6$; $\theta_{2s} = 0.2$; $Đ_1(0) = 10^{-14}\,m^2\,s^{-1}$; $\delta = 2\,\mu m$. Symbols represent precise numerical solutions obtained using the numerical techniques described on our website: http://ct-cr4.chem.uva.nl/zeolites/. The continuous lines are drawn using Eq. (28), with definitions of Φ as in Table 1.

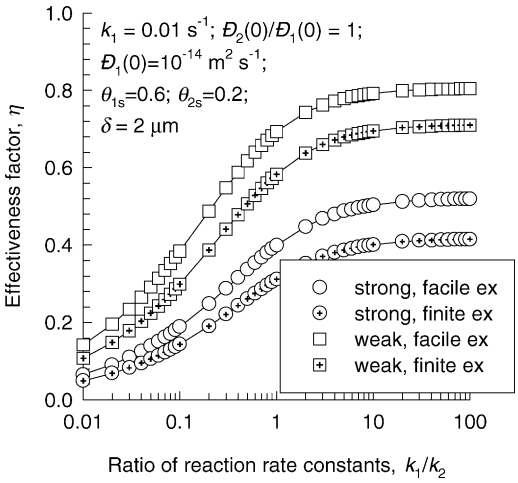

Fig. 7. Effectiveness factor η for varying ratios of reaction rate constants. Other parameters for the spherical catalyst geometry are $k_1 = 0.01\,s^{-1}$; $\theta_{1s} = 0.6$; $\theta_{2s} = 0.2$; $Đ_1(0) = Đ_2(0) = 10^{-14}\,m^2\,s^{-1}$; $\delta = 2\,\mu m$. The calculations are based on Eq. (28), with definitions of Φ as in Table 1.

the influence of exchange is only very minor. This conclusion is strengthened when we examine the variation of the effectiveness factor with the classical Thiele modulus ϕ in Fig. 5b; the differences between finite and facile exchange scenarios are hardly distinguishable. The effectiveness factor for strong confinement is significantly lower than for the case with weak confinement. Also plotted in Fig. 5b is the "classical" value of η, obtained by assuming $\Phi = \phi$, i.e. taking all other correction factors, β, Ξ, Ψ, and Θ to be unity. The classical case yields the highest η value, slightly higher than for facile exchange and weak confinement. The conclusion to be drawn from Fig. 5b is that it is not "safe" to use the classical approach for η when the molecules are strongly confined.

For a diffusivity ratios $Đ_2(0)/Đ_1(0)$ varying from 0.01 to 100, the η values for various scenarios are shown in Fig. 6. The "classical" value of η, obtained by assuming $\Phi = \phi$ is close to the weak confinement–facile exchange scenario; indeed for $Đ_2(0)/Đ_1(0) = 1$, these two calculations coincide as already remarked in the foregoing discussions. With increasing values of $Đ_2(0)/Đ_1(0)$ the differences between facile and finite exchange scenarios increase, and the η tend to reach nearly constant values.

A similar picture emerges when we vary the reaction equilibrium constant, described by the ratio of rate constants, k_1/k_2; see Fig. 7. When k_1/k_2 values exceed say 10, the isomerization can be considered to be practically irreversible and the η value is virtually constant, but confinement scenario dependent.

A further distinguishing feature of zeolite diffusion is that effectiveness factor is a function of the *composition* of the mixture. In Fig. 8, we show the variation of η with varying values of $\theta_{1s}/(\theta_{1s}+\theta_{2s})$ for three different diffusivity ratios:

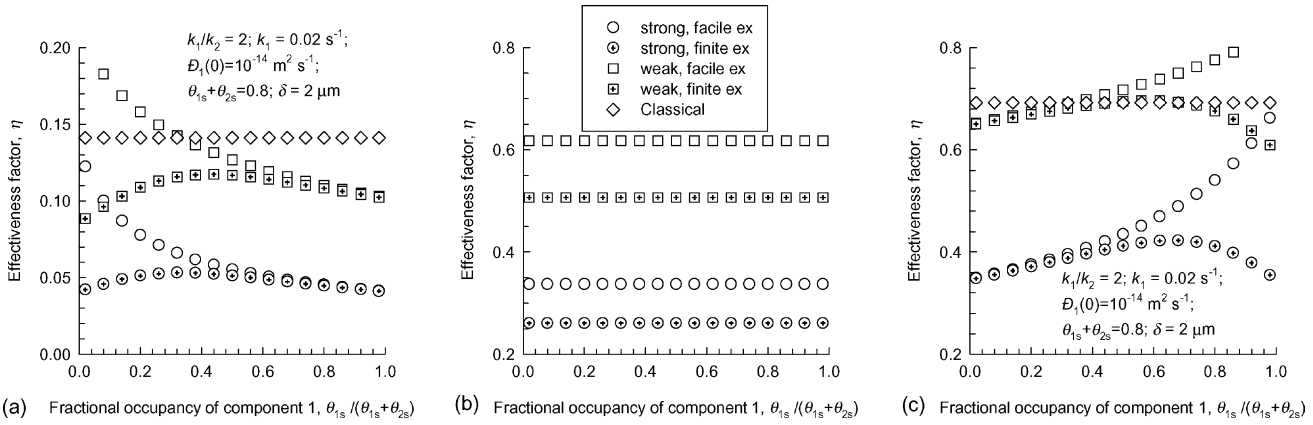

Fig. 8. Effectiveness factor η for varying compositions at the surface $\theta_{1s}/(\theta_{1s}+\theta_{2s})$ for (a) $Đ_2(0)/Đ_1(0) = 0.01$, (b) $Đ_2(0)/Đ_1(0) = 1$, and (c) $Đ_2(0)/Đ_1(0) = 100$. Other parameters for the spherical catalyst geometry are $k_1 = 0.02\,s^{-1}$; $\theta_{1s}+\theta_{2s} = 0.8$; $Đ_{1(0)=10^{-14}}\,m^2\,s^{-1}$; $\delta = 2\,\mu m$. The calculations are based on Eq. (28), with definitions of Φ as in Table 1.

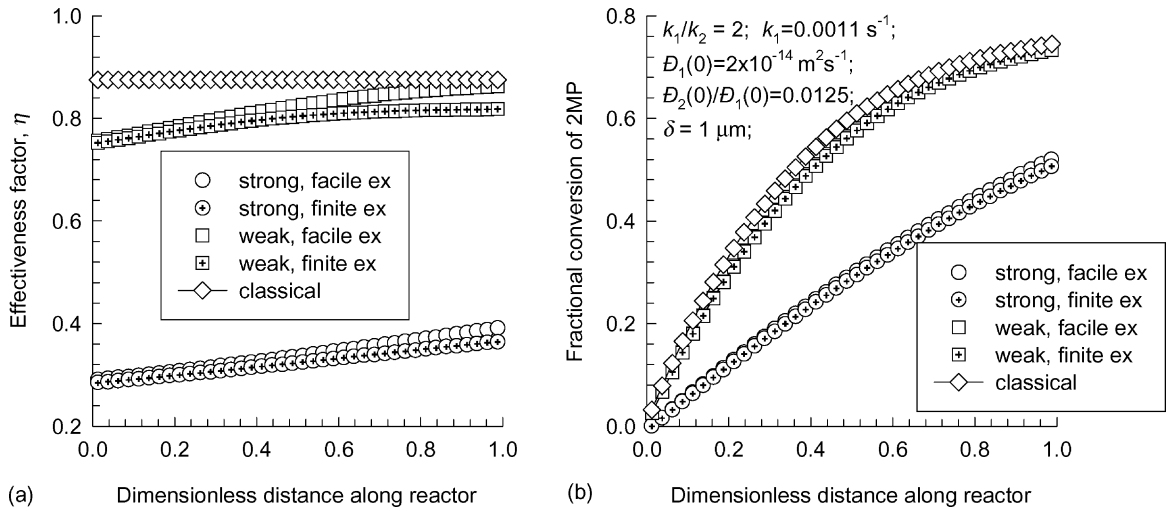

Fig. 9. (a) Effectiveness factor η and (b) 2MP conversion along reactor length. The reaction considered is the isomerization of 2MP to 22DMB with zeolite catalyst. Other parameters are as defined in Table 2.

(a) $Đ_2(0)/Đ_1(0) = 0.01$, (b) $Đ_2(0)/Đ_1(0) = 1$, and (c) $Đ_2(0)/Đ_1(0) = 100$. For $Đ_2(0)/Đ_1(0) = 0.01$ and facile exchange, the η value decreases with increasing composition of A_1; this effect is to be ascribed to the correction factor Ψ that increases with increasing proportion of A_1. Interestingly, the η value exhibits a maximum value for the finite exchange case. For $Đ_2(0)/Đ_1(0) = 1$, we have $\Lambda = 1$; $\Psi = 1$ and there is no composition influence. The η value is dictated by $\phi\Xi \equiv \phi\sqrt{[(1+\theta_{1s}+\theta_{2s})/(1-\theta_{1s}-\theta_{2s})^{\gamma}]}$, depending only on the total occupancy level and not on composition.

For $Đ_2(0)/Đ_1(0) = 100$ and facile exchange, the η value increases with increasing composition of A_1, due to the dependence of Ψ on composition. For finite exchange, the maximum in η is again evident.

All the illustrative examples considered above pertain to conditions within a single zeolite catalyst particle. In an actual reactor the compositions and occupancies will vary along the reactor, and therefore the effectiveness factor will also vary. Let us consider the specific example of isomerization of 2-methylpentane (2MP) to its dibranched isomer 2,2 dimethylbutane (22DMB) in a packed bed reactor. The reaction conditions, and parameters are specified in Table 2; the parameters are taken from the recent paper by Jolimaitre et al. [30]. The macropore diffusion resistance is not considered and the only intra-crystalline diffusion resistance is taken into account. The effectiveness factor along the reactor length is shown in Fig. 9a. The classical $\eta-\phi$ calculation yields a constant η value of 0.875 along the reactor and the 2MP conversion at the reactor exit is 0.745 (see Fig. 9b). The catalyst effectiveness is slightly lower for the weak confinement scenario; the influence of exchange coefficient is minimal. The reactor conversion at the exit is 0.735 for weak confinement. There is a significant reduction in η for strong confinement and fractional conversion of 2MP at the reactor exit is only 0.51.

Table 2
Pure component Langmuir parameters and M–S diffusivities for 2MP and 22DMB in zeolite packed bed reactor operating at 473 K

	2MP	22DMB
Saturation loading, q_{sat} (mol kg^{-1})	4	4
Langmuir parameter, b (Pa^{-1})	1.27×10^{-4}	7.12×10^{-5}
M–S diffusivity of pure components, $Đ_i(0)$ (m^2 s^{-1})	2×10^{-14}	2.5×10^{-16}
Length of bed, L (m)	0.798	
Crystallite radius, r_c (μm)	1	
Forward reaction rate constant, k_1 (s^{-1})	0.0011	
Reaction equilibrium constant, k_1/k_2	2	
Packed bed voidage (–)	0.4	
Partial pressures of 2MP and 22DMB at inlet (Pa)	10^5, 0.01	
Gas velocity at inlet (m s^{-1})	0.009	
Crystal density, ρ (kg m^{-3})	620.8	

Data from Jolimaitre et al. [30]. Also given are the parameters of the packed bed.

5. Conclusions

The major new contribution of this paper is the development of an analytic solution for diffusion with reversible isomerization reaction $A_1 \leftrightarrow A_2$, within a zeolite catalyst. Two extreme cases of occupancy dependence of the M–S diffusivities, weak and strong confinement, are taken into account. Furthermore, correlation effects typical of zeolite diffusion are catered for by the introduction of the exchange coefficient $Đ_{12}$ in the M–S diffusion formulation. The analytic solutions, given by Eq. (27) for the vacancy profile and Eq. (28) for η, have the same *form* as the classic solutions given in the literature [28]. The modified Thiele modulus Φ is related to the classic Thiele modulus ϕ in the manner outlined in Table 1 for various scenarios. The accuracy of the analytic solution is verified by comparison with precise numerical calculations.

By means of several illustrative examples we have underlined the peculiarities of zeolite diffusion, encapsulated in the various dimensionless parameters β, Ξ, Ψ, and Θ. The classical $\eta-\phi$ calculation is a good approximation only for weakly confined molecules with facile exchange between the two species. For strongly confined molecules, the η value is significantly lower the classical value and the obtained reactor conversion can be expected to significantly reduced.

Further work is required to extend the analysis to multicomponent systems and more general reaction schemes.

Acknowledgements

R.B. and R.K. acknowledge a grant *Programmasubsidie* from the The Netherlands Foundation for Fundamental Research (CW-NWO) for development of novel concepts in reactive separations.

Appendix A. Solution for strong confinement ($\gamma = 1$)

For strong confinement, $\gamma = 1$ the differential Eq. (25) simplify to yield

$$\frac{1}{\xi^{\zeta-1}}\frac{\partial}{\partial\xi}\left(\xi^{\zeta-1}\frac{\partial(\theta_V/\theta_{Vs})}{\partial\xi}\right) = (\zeta\Phi)^2\left(\frac{\theta_V}{\theta_{Vs}} - \frac{1}{\Psi^2}\right) \quad \text{(A.1)}$$

where the modified Thiele modulus $\Phi = \phi\beta\Xi\Psi$. The differential Eq. (A.1) is similar to the classical form for diffusion and reaction [28] and the solution for the vacancy profiles can be derived in an analogous manner for slab ($\zeta = 1$), cylindrical ($\zeta = 2$) and spherical ($\zeta = 3$) geometries:

$$\begin{aligned}
\frac{\theta_V}{\theta_{Vs}} &= \frac{1}{\Psi^2} + \left(\frac{\Psi^2-1}{\Psi^2}\right)\frac{\cosh(\Phi\xi)}{\cosh(\Phi)}; \quad \text{slab}(\zeta=1)\\
\frac{\theta_V}{\theta_{Vs}} &= \frac{1}{\Psi^2} + \left(\frac{\Psi^2-1}{\Psi^2}\right)\frac{I_0(2\Phi\xi)}{I_0(2\Phi)}; \quad \text{cylinder}(\zeta=2)\\
\frac{\theta_V}{\theta_{Vs}} &= \frac{1}{\Psi^2} + \left(\frac{\Psi^2-1}{\Psi^2}\right)\frac{\sinh(3\Phi\xi)}{\sinh(3\Phi)}; \quad \text{sphere}(\zeta=3)
\end{aligned} \quad \text{(A.2)}$$

The effectiveness factor is obtained from the defining equation:

$$\eta = \frac{\int_0^1 r\xi^{\zeta-1}\,d\xi}{\int_0^1 r|_{\xi=1}\xi^{\zeta-1}\,d\xi} = \zeta\frac{\int_0^1(1-\Psi^2(\theta_V/\theta_{Vs}))\xi^{\zeta-1}\,d\xi}{1-\Psi^2} \quad \text{(A.3)}$$

and the classical results for η given in Eq. (28) are recovered.

Appendix B. Solution for equal diffusivities

For the special case in which the two isomers have the same M–S diffusivity, the following simplifications result:

$$\begin{aligned}
&Đ_1(0) = Đ_2(0); \quad \beta \equiv 1; \quad \Lambda \equiv 1; \quad \Psi \equiv 1;\\
&r = k_1\theta_1 - k_2\theta_2 = (k_1+k_2)\theta_1 - k_2(1-\theta_{Vs})
\end{aligned} \quad \text{(B.1)}$$

and, therefore for the equimolar isomerization ($N_1 = -N_2$) under consideration in this paper Eq. (12) simplifies to yield

$$\sum_{i=1}^{n}\frac{N_i\delta}{\rho q_{sat}Đ_i(0)} = 0 = -\theta_V^{\gamma-1}\frac{\partial\theta_V}{\partial\xi} \quad \text{(B.2)}$$

which implies that the vacancy is constant along the diffusion path. As a consequence, we must have the partial pressures proportional to the loadings

$$\theta_V = \theta_{Vs}; \quad \pi_i = \frac{\theta_i}{\theta_{Vs}}; \quad \frac{\partial\theta_1}{\partial\xi} = -\frac{\partial\theta_2}{\partial\xi}; \quad i = 1,2 \quad \text{(B.3)}$$

and so Eq. (A.1) simplifies to

$$\frac{1}{\xi^{\zeta-1}}\frac{\partial}{\partial\xi}\left(\xi^{\zeta-1}\frac{\partial(\theta_1/\theta_{1s})}{\partial\xi}\right) = (\zeta\Phi)^2\left(\frac{\theta_1}{\theta_{1s}} - \frac{1}{\omega}\right) \quad \text{(B.4)}$$

where the modified Thiele modulus case is $\Phi = \phi\Xi$.

The occupancy profiles can be written in a manner analogous to Eq. (A.2) and the results are:

$$\begin{aligned}
\frac{\theta_1}{\theta_{1s}} &= \frac{1}{\omega} + \left(\frac{\omega-1}{\omega}\right)\frac{\cosh(\Phi\xi)}{\cosh(\Phi)}; \quad \text{slab}(\zeta=1)\\
\frac{\theta_1}{\theta_{1s}} &= \frac{1}{\omega} + \left(\frac{\omega-1}{\omega}\right)\frac{I_0(2\Phi\xi)}{I_0(2\Phi)}; \quad \text{cylinder}(\zeta=2)\\
\frac{\theta_1}{\theta_{1s}} &= \frac{1}{\omega} + \left(\frac{\omega-1}{\omega}\right)\frac{\sinh(3\Phi\xi)}{\sinh(3\Phi)}; \quad \text{sphere}(\zeta=3)
\end{aligned} \quad \text{(B.5)}$$

with effectiveness factors η given by Eq. (28) for the three geometries.

Appendix C. Solution for weak confinement ($\gamma = 0$)

The derivation for the solution for weak confinement can be derived for the slab geometry using the classical work of Ruthven [13]; this paper along with the book of Aris [28] is used as a guide in the derivation given below for all geometries. The general differential Eq. (25) simplifies to yield:

$$\frac{\partial}{\partial\xi}\left(\frac{1}{\theta_V/\theta_{Vs}}\frac{\partial(\theta_V/\theta_{Vs})}{\partial\xi}\right) = (\phi\beta\Xi\Psi)^2\left(\frac{\theta_V}{\theta_{Vs}} - \frac{1}{\Psi^2}\right) \quad \text{(C.1)}$$

We substitute

$$\frac{1}{\theta_V/\theta_{Vs}}\frac{\partial(\theta_V/\theta_{Vs})}{\partial\xi} = \chi; \quad \frac{\theta_V}{\theta_{Vs}} = \frac{1}{\chi}\frac{\partial(\theta_V/\theta_{Vs})}{\partial\xi} \quad \text{(C.2)}$$

to obtain

$$\begin{aligned}
\chi\frac{\partial\chi}{\partial\xi} &= (\phi\beta\Xi\Psi)^2\left(\frac{\partial(\theta_V/\theta_{Vs})}{\partial\xi} - \frac{1}{\Psi^2}\chi\right)\\
&= (\phi\beta\Xi\Psi)^2\left(1 - \frac{1}{\Psi^2}\frac{1}{(\theta_V/\theta_{Vs})}\right)\frac{\partial(\theta_V/\theta_{Vs})}{\partial\xi}
\end{aligned} \quad \text{(C.3)}$$

Integrating Eq. (C.3) we obtain

$$\int_{\xi=0}^{\xi} \chi \frac{\partial \chi}{\partial \xi}\, \mathrm{d}\xi = \int_{\xi=0}^{\xi} (\phi\beta\Xi\Psi)^2 \left(1 - \frac{1}{\Psi^2}\frac{1}{(\theta_V/\theta_{Vs})}\right) \frac{\partial(\theta_V/\theta_{Vs})}{\partial\xi}\, \mathrm{d}\xi \tag{C.4}$$

whose solution can be written down as

$$\chi = \pm\sqrt{2}\phi\beta\Xi\Psi \left(\left(\frac{\theta_V}{\theta_{Vs}} - \frac{\theta_{V0}}{\theta_{Vs}}\right) - \frac{1}{\Psi^2}\left(\ln\left(\frac{\theta_V}{\theta_{Vs}}\right) - \ln\left(\frac{\theta_{V0}}{\theta_{Vs}}\right)\right)\right)^{1/2} \tag{C.5}$$

where θ_{V0} is the vacancy at the center of the slab ($\xi = 0$). In order to estimate the vacancy at the center of the slab, we assume chemical equilibrium, i.e. $r = 0$. This assumption of chemical equilibrium is expected to be hold for low effectiveness factors, say $\eta < 0.5$. From Eqs. (14), (21) and (22) we obtain

$$\frac{\theta_{10}}{\theta_{20}} = \frac{k_2}{k_1}; \qquad \frac{\theta_{V0}}{\theta_{Vs}} = \frac{(k_2 + \Lambda k_1)}{(\Lambda + (1-\Lambda)\theta_{1s})k_1 + (1 + (\Lambda - 1)\theta_{2s})k_2} = \frac{1}{\Psi^2} \tag{C.6}$$

Combining Eqs. (C.5) and (C.6) yields

$$\chi = \pm\sqrt{2}(\phi\beta\Xi\Psi) \left(\left(\frac{\theta_V}{\theta_{Vs}} - \frac{1}{\Psi^2}\right) - \frac{1}{\Psi^2}\left(\ln\left(\frac{\theta_V}{\theta_{Vs}}\right) - 2\ln(\Psi)\right)\right)^{1/2} \tag{C.7}$$

The effectiveness factor for the slab geometry is defined by

$$\eta = \frac{\int_0^1 r(\xi)\, \mathrm{d}\xi}{r|_{\xi=1}} = \frac{\chi|_{\xi=1} - \chi|_{\xi=0}}{(\phi\beta\Xi\Psi)^2(1 - \Psi^{-2})} \tag{C.8}$$

Combining Eqs. (C.7) and (C.8) results in the following expression for the effectiveness factor

$$\eta = \frac{\Theta}{\phi\beta\Xi\Psi}; \qquad \Theta \equiv \frac{\sqrt{2(1 - (1/\Psi^2) - 2\ln(\Psi)/\Psi^2)}}{|1 - 1/\Psi^2|} \tag{C.9}$$

Since the derivation of Eq. (C.9) was on the basis of low effectiveness factor $\eta < 0.5$, we can conclude from Eq. (29) that the *effective* Thiele modulus Φ for weak confinement is

$$\Phi = \frac{\phi\beta\Xi\Psi}{\Theta} \tag{C.10}$$

The following formula for the effectiveness factor derived by Ruthven [13]:

$$\eta = \frac{\sqrt{2(-\theta_{1s} - \ln(1 - \theta_{1s}))}}{\phi\sqrt{(1 - \theta_{1s})}\theta_{1s}} \tag{C.11}$$

can be recovered from Eq. (C.9) by making the additional assumptions: (a) the fractional loading of the product at the surface is vanishingly small, i.e. $\theta_{2s} \to 0$, and (b) diffusion of the product is infinitely fast, $Đ_2(0) \to \infty$.

References

[1] D.M. Ruthven, Principles of Adsorption and Adsorption Processes, Wiley, New York, 1984.
[2] J. Kärger, D.M. Ruthven, Diffusion in Zeolites and other Microporous Solids, Wiley, New York, 1992.
[3] A. Corma, State of the art and future challenges of zeolites as catalysts, J. Catal. 216 (2003) 298–312.
[4] J. Degnan, F. Thomas, The implications of the fundamentals of shape selectivity for the development of catalysts for the petroleum and petrochemical industries, J. Catal. 216 (2003) 32–46.
[5] C. Marcilly, Present status and future trends in catalysis for refining and petrochemicals, J. Catal. 216 (2003) 47–62.
[6] C. Baerlocher, W.M. Meier, D.H. Olson, Atlas of Zeolite Framework Types, fifth ed., Elsevier, Amsterdam, 2002.
[7] D.M. Ruthven, M.F.M. Post, Diffusion in zeolite molecular sieves, in: H. van Bekkum, E.M. Flanigan, P.A. Jacobs, J.C. Jansen (Eds.), Introduction to Zeolite Science and Practice, vol. 137, Elsevier, Amsterdam, 2001, pp. 525–577 (Chapter 12).
[8] A.I. Skoulidas, D.S. Sholl, Direct tests of the darken approximation for molecular diffusion in zeolites using equilibrium molecular dynamics, J. Phys. Chem. B 105 (2001) 3151–3154.
[9] A.I. Skoulidas, D.S. Sholl, Transport diffusivities of CH4, CF4, He, Ne, Ar, Xe, and SF6 in silicalite from atomistic simulations, J. Phys. Chem. B 106 (2002) 5058–5067.
[10] A.I. Skoulidas, D.S. Sholl, R. Krishna, Correlation effects in diffusion of CH4/CF4 mixtures in MFI zeolite. A study linking MD simulations with the Maxwell–Stefan formulation, Langmuir 19 (2003) 7977–7988.
[11] A.I. Skoulidas, D.S. Sholl, Molecular dynamics simulations of self, corrected, and transport diffusivities of light gases in four silica zeolites to assess influences of pore shape and connectivity, J. Phys. Chem. B (2003), in press.
[12] J. Kärger, S. Vasenkov, S.M. Auerbach, Diffusion in zeolites, in: S.M. Auerbach, K.A. Carrado, P.K. Dutta (Eds.), Handbook of Zeolite Science and Technology, Marcel Dekker, New York, 2003, pp. 341–422 (Chapter 10).
[13] D.M. Ruthven, Effectiveness factor for molecular sieve catalysts, J. Catal. 25 (1972) 259–264.
[14] D.N. Theodorou, J. Wei, Diffusion and reaction in blocked and high occupancy zeolite catalysts, J. Catal. 83 (1983) 205–224.
[15] S. Sundaresan, C.K. Hall, Mathematical modelling of diffusion and reaction in blocked zeolite catalysts, Chem. Eng. Sci. 41 (1986) 1631–1645.
[16] R. Krishna, J.A. Wesselingh, The Maxwell–Stefan approach to mass transfer, Chem. Eng. Sci. 52 (1997) 861–911.
[17] F. Kapteijn, J.A. Moulijn, R. Krishna, The generalized Maxwell–Stefan model for diffusion in zeolites: sorbate molecules with different saturation loadings, Chem. Eng. Sci. 55 (2000) 2923–2930.
[18] R. Krishna, R. Baur, Modelling issues in zeolite based separation processes, Sep. Purif. Technol. 33 (2003) 213–254.
[19] B. Smit, R. Krishna, Molecular simulations in zeolitic process design, Chem. Eng. Sci. 58 (2003) 557–568.
[20] F.J. Keil, R. Krishna, M.O. Coppens, Modeling of diffusion in zeolites, Rev. Chem. Eng. 16 (2000) 71–197.
[21] E.J. Maginn, A.T. Bell, D.N. Theodorou, Transport diffusivity of methane in silicalite from equilibrium and nonequilibrium simulations, J. Phys. Chem. 97 (1993) 4173–4181.
[22] D. Paschek, R. Krishna, Monte Carlo simulations of self- and transport-diffusivities of 2-methylhexane in silicalite, Phys. Chem. Chem. Phys. 2 (2000) 2389–2394.

[23] D. Paschek, R. Krishna, Inter-relation between self- and jump-diffusivities in zeolites, Chem. Phys. Lett. 333 (2001) 278–284.
[24] R. Krishna, D. Paschek, Verification of the Maxwell–Stefan theory for tracer diffusion in zeolites, Chem. Eng. J. 85 (2002) 7–15.
[25] D. Paschek, R. Krishna, Monte Carlo simulations of sorption and diffusion of isobutane in silicalite, Chem. Phys. Lett. 342 (2001) 148–154.
[26] R. Krishna, D. Paschek, Self-diffusivities in multicomponent mixtures in zeolites, Phys. Chem. Chem. Phys. 4 (2002) 1891–1898.
[27] R. Krishna, Predicting transport diffusivities of binary mixtures in zeolites, Chem. Phys. Lett. 355 (2002) 483–489.
[28] R. Aris, The Mathematical Theory of Diffusion and Reaction in Permeable Catalysts, Clarendon Press, Oxford, 1975.
[29] H.A. Kooijman, Dynamic Nonequilibrium Column Simulations, Ph.D. Dissertation, Clarkson University, Potsdam, New York, 1995.
[30] E. Jolimaitre, K. Ragil, M. Tayakout-Fayolle, C. Jallut, Separation of mono- and dibranched hydrocarbons on silicalite, AIChE J. 48 (2002) 1927–1937.